JOURNAL OF GEOPHYSICAL RESEARCH, VOL. 106, NO. C4, PAGES 7125–7138, APRIL 15, 2001

A chlorophyll-dependent semianalytical reflectance model derived from field measurements of absorption and backscattering coefficients within the Southern Ocean

Rick A. Reynolds,[1] Dariusz Stramski, and B. Greg Mitchell

Scripps Institution of Oceanography, University of California San Diego, La Jolla, California

Abstract. A semianalytical model was developed for the prediction of spectral remote sensing reflectance (R_{rs}) as a function of fluorometric chlorophyll *a* concentration (Chl) for two regions within the Southern Ocean: the Ross Sea and the Antarctic Polar Front Zone (APFZ). The model is based upon Chl-dependent parameterizations of the spectral absorption, $a(\lambda)$, and backscattering, $b_b(\lambda)$, coefficients of seawater which were derived from field measurements. The relationships between $a(\lambda)$ and Chl were similar in both regions, but for comparable Chl the particulate backscattering was on average 4 times greater in the APFZ. Measurements of particle size distributions suggest that particle assemblages in the APFZ were characterized by a greater predominance of smaller particles, consistent with the observed regional differences in backscattering properties. The model is used to examine the separate influences of absorption and backscattering on the blue to green ratio of reflectance, $R_{rs}(490)/R_{rs}(555)$. Variability in the spectral absorption ratio, resulting principally from changes in the relative contribution of water to total absorption in each band, contributes >75% to changes in the $R_{rs}(490)/R_{rs}(555)$ ratio as a function of Chl. However, variability in the spectral backscattering ratio appears to be the primary cause for the observed differentiation in the R_{rs} versus Chl relationships between the two regions.

1. Introduction

The Southern Ocean is a quantitatively important component of global carbon and other biogeochemical cycles [*Sarmiento and Orr,* 1991; *Sarmiento et al.,* 1998]. Models to estimate fluxes and transformations of energy and materials in this region, and their susceptibility to perturbations in climate, require information on the time-varying distribution of phytoplankton biomass and rates of primary production. Because of the large area and relative inaccessibility of the Southern Ocean, as well as significant temporal and spatial variability in phytoplankton biomass, the remote sensing of near surface pigment concentrations provides the only practical means of obtaining large scale observations of phytoplankton distributions over appropriate timescales. The present availability of satellite ocean color data from the Sea-viewing Wide Field-of-view Sensor (SeaWiFS) and Moderate Resolution Imaging Spectrometer (MODIS), in addition to ocean color satellite missions to be launched in the near future, offers an unprecedented opportunity to force biogeochemical models with input from real time estimates of pigment distributions and to validate model behavior with observations.

Empirical algorithms for estimating surface pigment concentrations from satellites rely upon systematic variations between chlorophyll content and blue to green spectral ratios of the water-leaving radiance, $L_w(\lambda)$, where λ is light wavelength, or the remote sensing reflectance, $R_{rs}(\lambda)$, defined as L_w normalized to the downwelling plane irradiance incident upon the sea surface. Modern algorithms have been developed from the statistical analysis of large diverse data sets which contain simultaneous measurements of upper ocean optical properties and chlorophyll concentration [*O'Reilly et al.,* 1998]. However, measurements from polar waters, and from the Southern Ocean in particular, have not been well represented in these data sets despite the fact that they comprise a significant proportion of the total surface area of the ocean. Previous studies have provided evidence that bio-optical relationships in polar waters often deviate from those observed in low latitude systems [*Mitchell and Holm-Hansen,* 1991; *Mitchell,* 1992; *Arrigo et al.,* 1998], implying that specific regional parameterizations are necessary to obtain accurate pigment estimates in these locations.

The systematic deviation of ocean color relationships in the Southern Ocean from lower latitude waters suggests different relationships between absorption, backscattering, or both with chlorophyll concentration. Understanding natural variability in both absorption and backscattering coefficients and evaluating their influence on ocean color algorithms are therefore prerequisite for developing rational models which relate R_{rs} and pigment concentrations. During the past two decades, several in situ and in vitro methods have been developed for measuring the absorption coefficient of natural waters [e.g., *Pegau et al.,* 1995, and references therein]. Particulate absorption and its relationship to chlorophyll concentration has been the most extensively studied [*Garver et al.,* 1994; *Cleveland,* 1995; *Bricaud et al.,* 1998]. In contrast to absorption, there have been few in situ measurements of the

[1]Now at School of Oceanography, University of Washington, Seattle, Washington.

Paper number 1999JC000311.
0148-0227/01/1999JC000311$09.00

backscattering coefficient owing to a lack of appropriate instrumentation, and investigators have been forced to rely on backscattering models which could not be validated experimentally in the field. Only recently has instrumentation become commercially available for the estimation of spectral backscattering coefficients [*Maffione and Dana,* 1997].

We present results of concurrent measurements of remote sensing reflectance, backscattering, and absorption for two regions of the Southern Ocean, the Ross Sea and the Antarctic Polar Front Zone (APFZ). These measurements encompass a broad range of planktonic biomass, including waters dominated by the spring bloom of *Phaeocystis antarctica* within the Ross Sea. Variability in the inherent optical properties of seawater is described in terms of the chlorophyll *a* concentration as determined by fluorometry (Chl), and these relationships are used to develop a semianalytical forward model of remote sensing reflectance. The model covers the visible wavelength region 400 to 700 nm at 1-nm resolution and is used to generate a library of oceanic $R_{rs}(\lambda)$ spectra for the Ross Sea and the APFZ region. Comparing measured reflectance spectra with such a library provides a means to evaluate various chlorophyll algorithms for any number and combination of spectral bands that are available to the investigator. We demonstrate with this model how variability in absorption and backscattering relationships with Chl contributes to regional differentiation in empirical ocean color algorithms which utilize $R_{rs}(490)/R_{rs}(555)$ for the estimation of pigment concentrations.

2. Formulation of the Reflectance Model

The irradiance reflectance at null depth ($z = 0^-$) beneath the sea surface, $R(\lambda,0^-)$, is defined as the ratio of the upwelling, $E_u(\lambda,0^-)$, and downwelling, $E_d(\lambda,0^-)$, plane irradiances. Omitting the wavelength arguments for brevity, the remote sensing reflectance measured in the nadir direction just above the sea surface, $R_{rs}(0^+)$ is related to $R(0^-)$ through the relation [*Mobley,* 1994]

$$R_{rs}(0^+) = \frac{L_w(0^+)}{E_d(0^+)} = \left(\frac{(1-\rho_{wa})(1-r_{aw})}{n_w^2\,[1-r_{wa}R(0^-)]}\right)\left(\frac{R(0^-)}{Q}\right) \approx \kappa\left(\frac{R(0^-)}{Q}\right), \quad (1)$$

where $L_w(0^+)$ is the water-leaving radiance measured in the nadir direction just above the sea surface $z = 0^+$, $E_d(0^+)$ is the downwelling plane irradiance incident on the sea surface, ρ_{wa} is the Fresnel reflectance at the water-air interface for upwelling radiance normal to the sea surface, r_{aw} is the Fresnel reflectance at the air-water interface for downwelling irradiance, r_{wa} is the Fresnel reflectance at the water-air interface for upwelling irradiance, n_w is the refractive index of water, and Q is a factor representing the subsurface ratio of $E_u(\lambda,0^-)$ to the upwelling nadir radiance, $L_u(\lambda, 0^-)$. The Fresnel reflectance coefficients vary with sea state but are only weakly dependent on wavelength [*Austin,* 1974], and the value of R is generally small (< 0.1) in most oceanic waters; thus the combination of terms contained in the first brackets can be approximated by a constant κ.

Both $R(\lambda,0^-)$ and $R_{rs}(\lambda,0^-)$ are so-called apparent optical properties (AOP) as they are dependent upon the directional structure of the radiance distribution in addition to the optical characteristics of the medium [*Preisendorfer,* 1961]. Numerical modeling studies have shown that the subsurface reflectance at any wavelength can be related to the absorption, $a(\lambda)$, and backscattering, $b_b(\lambda)$, coefficients of seawater through the approximation [*Gordon et al.,* 1988]

$$\frac{R(0^-)}{Q} \equiv \frac{L_u(0^-)}{E_d(0^-)} \approx \left(\frac{f}{Q}\right)\left(\frac{b_b}{a+b_b}\right), \quad (2)$$

where f is a variable factor that depends upon the incoming radiance distribution, the optical properties of seawater, and light wavelength [*Morel and Gentili,* 1991, 1993]. The absorption and backscattering coefficients (inherent optical properties (IOP)) are independent of the radiance field and can be partitioned into the cumulative sum of individual contributions by optically significant constituents of seawater such as water molecules, particulate matter, and colored dissolved organic material (CDOM):

$$a(\lambda) = a_w(\lambda) + a_p(\lambda) + a_{cdom}(\lambda) \quad (3)$$

$$b_b(\lambda) = b_{bw}(\lambda) + b_{bp}(\lambda)\,. \quad (4)$$

We assume that the contribution of dissolved materials to backscattering is negligible and that the contribution of water to the absorption and backscattering coefficients at any light wavelength can be considered constant. In regions such as the Southern Ocean which are generally isolated from terrigenous sources, variability in both the backscattering and absorption coefficients are largely determined by changes in the concentrations and composition of the suspended particle assemblage. Variability in ocean reflectance thus contains information on the planktonic community present and on the ecological processes driving changes in the concentration of individual constituents.

We have utilized equations (1) through (4) in combination with field measurements to develop a semianalytical model for the prediction of spectral remote sensing reflectance as a function of surface Chl for two regions of the Southern Ocean. Concurrent measurements of Chl, the absorption by particles and CDOM (equation (3)), and the total backscattering coefficient of seawater (equation (4)) are used to develop regional parameterizations of the inherent optical properties, and these parameterizations are used to drive a forward model of reflectance which has the basic form

$$R_{rs}(\lambda, 0^+, \mathrm{Chl}) = 0.54\left(\frac{f(\lambda)}{Q(\lambda)}\right)\left(\frac{b_b(\lambda,\mathrm{Chl})}{a(\lambda,\mathrm{Chl})+b_b(\lambda,\mathrm{Chl})}\right), \quad (5)$$

where the dependence of a, b_b, and R_{rs} on Chl is made explicit, and we assume a constant, spectrally independent value of $\kappa = 0.54$.

We next describe the measurements and data used to formulate the model parameterizations of the inherent optical properties. The spectral behavior of the ratio f/Q is then determined by comparing independent measurements of the directional reflectance, $L_u(\lambda,0^-)/E_d(\lambda,0^-)$, with concurrent measurements of the backscattering and absorption coefficients (equation (2)).

3. Measurement and Parameterization of Model Components

3.1. Bio-Optical Field Measurements

Field measurements were obtained in the Ross Sea and the Antarctic Polar Front Zone (APFZ) as part of the U.S. Joint Global Ocean Flux Study (JGOFS) within the Southern Ocean

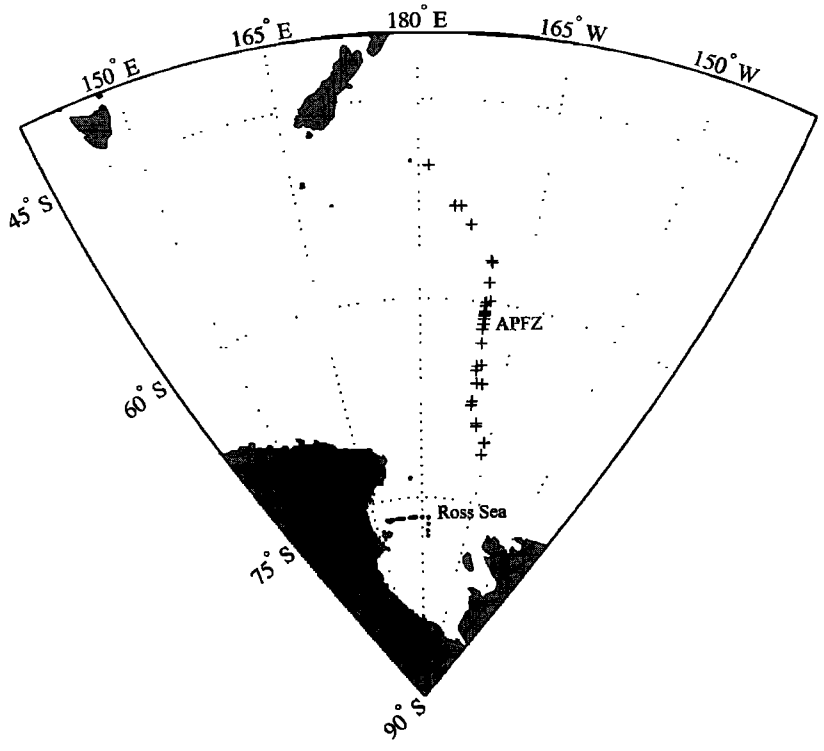

Figure 1. Map of study region and stations occupied in the Ross Sea (solid circles) and in the Antarctic Polar Front Zone (APFZ, plus signs) as part of the U.S. Joint Global Ocean Flux Study within the Southern Ocean.

[*Smith et al.*, 2000]. The Ross Sea cruise took place during November and December 1997 and repetitively sampled a main latitudinal transect along 76.5°S (169°E–178°W) throughout the development of the annual spring bloom (Figure 1). Two summer cruises, covering the period January through March 1998, examined longitudinal variations across the APFZ along 170°W between 50°S and 72°S (Figure 1).

Surface waters in the study regions were generally well mixed within the first optical depth, and profiles of the inherent optical properties within this layer were often uniform. Because our present interests lie in relating inherent optical properties to surface reflectance, we restrict our data set to measurements obtained in the upper 15 m of the water column. This geometric depth represents the average penetration depth at 490 nm ($1/K_d$ [*Gordon and Morel*, 1983]) for all stations, and this portion of the water column is the dominant source (~90%) of the water-leaving radiance.

3.1.1. In situ optical profiles. A submersible optical profiling system was used to obtain vertical profiles of apparent and inherent optical properties in the upper 200 m of the water column. The system consisted of a MER-2040 spectroradiometer (Biospherical Instruments) measuring downwelling spectral irradiance and upwelling radiance for 13 spectral bands within the wavelength range 340-700 nm. The optical characterization and radiometric calibration history for this instrument is described in greater detail elsewhere [*Mitchell and Kahru*, 1998]. The MER-2040 was interfaced with two 25-cm beam transmissometers (488 and 660 nm, WetLabs), a stimulated chlorophyll fluorometer (WetLabs), and conductivity and temperature probes (SeaBird). Spectral backscattering measurements were obtained for six spectral bands (442, 470, 510, 589, 620, and 671 nm) with a Hydroscat-6 backscattering meter (Hobi Labs).

All instruments were integrated into a black stainless steel frame, with power and data acquisition controlled by a WetLabs Modular Data and Power System and transmitted through the ship's hydrographic conducting cable. The instrument package was deployed over the side of the ship in accordance with recommended SeaWiFS bio-optical protocols [*Mueller and Austin*, 1995].

To minimize errors in matching depths between the optical profiling package and water samples collected from the conductivity-temperature-depth (CTD) rosette system, distinct features in conductivity, temperature, and beam transmission which remained consistent between casts were used to correct the depth sensor of the optical package relative to the CTD. Radiometric data were processed using the Bermuda Bio-Optics Project (BBOP) system [*Siegel et al.*, 1995] as modified by *Mitchell and Kahru* [1998]. Individual profiles were split into separate downcast and upcast, and the data from each channel were binned into 1-m depth intervals. Profiles were visually inspected for quality (e.g. minimal ship shadow effect, uniformity of features), and a depth range within the upper mixed layer was selected for extrapolation of radiometric quantities to immediately beneath the sea surface.

The Hydroscat-6 provides a quantitative measure of the volume scattering function at a fixed scattering angle centered near 140°, which can be related to the total backscattering coefficient. The methodology of this measurement, calibration procedures, and subsequent determination of the backscattering coefficient are described in detail by *Maffione and Dana* [1997]. Beam attenuation coefficients measured in situ with the two beam transmissometers were interpolated to match the Hydroscat-6 wavebands and used to correct the backscattering measurements for attenuation effects. The magnitude of this correction is small in these waters, typically 2 to 3% of

the measured signal. Backscattering data collected at the six specific wavebands of the Hydroscat-6 were fit to a spectral power law for extrapolation to wavelength regions that matched the MER-2040 spectroradiometer.

3.1.2. Discrete water sample analyses. Water samples at discrete depths were collected from one of two CTD rosette systems employed by the JGOFS program [*Knap et al.*, 1994]. The first system included twenty-four 10-*l* Niskin bottles mounted on a rosette frame coated with an inert plastic resin to minimize trace metal contamination. The second system, used principally for productivity measurements, consisted of a trace metal clean rosette containing eight 30-*l* Go-Flo Niskin bottles. For correlation analyses with optical data, only water samples collected from CTD casts immediately prior to or following optical profiles were used. Under such conditions, the time offset between collection of water samples and acquisition of in situ optical data was generally less than 1.5 hours.

3.1.2.1. Pigments: Pigment concentrations were quantified by using standard JGOFS protocols [*Knap et al.*, 1994]. Water samples were concentrated by filtration onto 25-mm Whatman glass fiber filters (GF/F) under low vacuum, extracted 24 hours in 90% acetone, and chlorophyll and pheopigment concentrations of the extract were determined fluorometrically with a Turner Designs model 10-AU fluorometer.

Additional samples were taken on all cruises for analysis of pigments by high-performance liquid chromatography (HPLC). Chl derived from HPLC was calculated as the sum of chlorophyll *a* plus derivatives (chlorophyllide *a*, chlorophyll *a* allomers and epimers) and compared with fluorometrically determined values. For the Ross Sea cruise, HPLC and fluorometric Chl values were highly correlated and yielded an average agreement within 15% with no systematic deviation between the two estimates. HPLC and fluorometric values were also strongly correlated for the two APFZ cruises, but fluorometric values were significantly higher in comparison with HPLC-determined Chl. No instrumental or analytical cause for this discrepancy has been identified. For the subset of APFZ Chl data relevant to the present manuscript in which concurrent measurements of HPLC are available, regression analysis (model II) yielded the relationship Chl(fluorometric) = 1.69 Chl(HPLC) + 0.10 ($r^2 = 0.96$, $N = 46$).

Controlled laboratory studies have observed that the fluorometric method tends to overestimate HPLC-determined chlorophyll [*Neveux et al.*, 1990], and field studies suggest these disparities can vary significantly in space and time [e.g., *Trees et al.*, 1986; *Bianchi et al.*, 1995]. In the present case, the use of HPLC values for the APFZ result in chlorophyll-specific absorption coefficients of phytoplankton which are not easily reconcilable with current understanding of this quantity, as the values at the red peak of chlorophyll *a* appear to be too high (significantly greater than 0.03 m^2 (mg Chl)$^{-1}$, reaching values as high as 0.15 m^2 (mg Chl)$^{-1}$). Because of these uncertainties, and to remain consistent with most previous studies regarding chlorophyll-specific absorption by phytoplankton, we have chosen to utilize fluorometric Chl data to parameterize our bio-optical model for reflectance without attempting to reconcile the two measurements by an empirical correction. Thus all Chl data used in the present paper represent fluorometric values.

3.1.2.2. Particle and soluble absorption: Spectral absorption coefficients (300-800 nm) of particulate, $a_p(\lambda)$, and colored dissolved organic material, $a_{cdom}(\lambda)$, were measured on freshly collected samples in a Cary 1E dual-beam spectrophotometer (Varian Instruments). Particulate matter was collected by filtration with low vacuum onto 25-mm Whatman GF/F, stored on ice, and scanned within 18 hours of collection. A blank filter saturated with filtered seawater was used as the reference. Optical density of the sample filters were converted to spectral absorption coefficients by using the procedure outlined by *Mitchell* [1990]. During the Ross Sea cruise, experiments were performed at four stations to examine the pathlength amplification caused by multiple scattering occurring within the filter. Based upon these measurements, the algorithm of *Mitchell* [1990] was chosen as providing a reasonably good correction for this effect. Following determination of $a_p(\lambda)$, sample filters were extracted 1 hour in 100% methanol and remeasured to yield experimental estimates of detrital absorption [*Kishino et al.*, 1985]. We note that in this context, detrital absorption is operationally defined as that component of particulate absorption which is not attributed to pigments that are extractable in methanol.

The absorption of CDOM was determined by measurements of 0.2-μm seawater filtrates (Nuclepore) in 10-cm pathlength quartz cuvettes. Filters were soaked in 10% HCl for >15 min and rinsed with Milli-Q water before sample filtration to minimize the absorption by material leached from the filters. Milli-Q water, freshly prepared at the time of measurement, was used as the reference. As CDOM absorption is often extremely low in these waters, the measurements are sensitive to instrument noise, baseline variability, slight temperature offsets between the sample and reference, and scattering error introduced by particles passing through the filter. To minimize these potential errors, raw spectra were normalized to yield zero absorption in the wavelength region 590-600 nm and subsequently fit to a spectral power law for use in later calculations (see equation (7)).

3.1.2.3. Particle size distributions: Particle size distributions were measured on discrete water samples with a Coulter counter model TAII equipped with a 100-μm aperture and coupled with a Coulter Multisizer IIE. In this configuration, particle number per unit volume, *N/V*, was obtained in 256 discrete size classes covering the approximate size range 2 to 63 μm. These concentrations are expressed as the number of particles per unit volume within each size class, where each discrete class has a width of 0.25 μm. The instrument was calibrated with latex microspheres (Coulter Instruments), with freshly prepared filtered seawater (0.22 μm) used as the blank. Triplicate measurements of the size distribution were made on each sample, and the results were combined to yield the final size distribution.

3.2. Surface Chlorophyll and Particle Size Distributions

Within the Ross Sea, substantial mesoscale variability in the extent of ice cover was encountered throughout the cruise. During the initial survey of the study area, heavy ice cover remained and surface Chl was uniformly low. As the season progressed, mixed layer depths decreased as a result of melting ice and, in conjunction with increasing levels of solar radiation, resulted in a rapid increase and accumulation of phytoplankton biomass. This process culminated with a large bloom of the Prymnesiophyte *Phaeocystis antarctica* in the

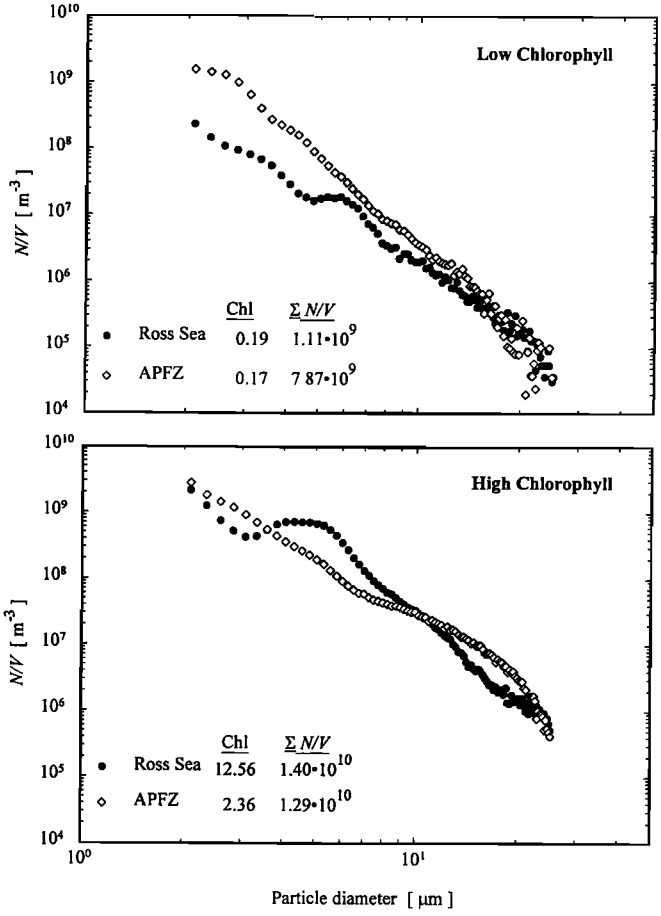

Figure 2. Particle size distributions for the Ross Sea and Antarctic Polar Front Zone as determined from Coulter counter measurements. (top) Representative stations with low surface chlorophyll. (bottom) Stations at which the maximum chlorophyll was observed in each region. The concentration of chlorophyll (Chl, mg m^{-3}) and the summed particle concentration over the measured size range ($\Sigma N/V$, m^{-3}) are indicated for each station.

western region of the study area during early December, with Chl exceeding 14 mg m^{-3}. Pheopigment concentrations in surface waters ranged from 0.05 to 3.5 mg m^{-3} and were highly correlated with Chl ($r = 0.90$, $N = 253$).

The Antarctic Polar Front Zone is a major oceanographic feature encircling the Antarctic continent. SeaWiFS imagery of this region discerned elevated chlorophyll concentrations (>2 mg m^{-3}) occurring near the vicinity of the Polar Front during austral spring and summer [*Moore et al.*, 1999]. By the period in which our measurements were conducted, these blooms had dissipated and only small isolated remnants of elevated Chl remained. The maximum Chl encountered in our measurements within the APFZ was about 2.5 mg m^{-3}.

Comparison of size distribution measurements suggests that particle assemblages in the APFZ were characterized by a greater predominance of smaller particles as compared to the Ross Sea. Figure 2 illustrates representative size distributions measured within each region. For clear water stations (Chl < 0.2 mg m^{-3}), particle concentrations within the measured size range were about sevenfold higher in the APFZ, with the greatest differences occurring in the smaller size classes. Particle concentrations increased at stations representing the highest Chl encountered in each region, but it is remarkable that despite a fivefold greater Chl observed in the Ross Sea, the integrated particle concentrations are comparable. The Ross Sea distributions are characterized by a conspicuous peak in the 4 to 6 μm range, corresponding to the general size range of individual *Phaeocystis* cells. These results suggest that the APFZ is more similar to typical open ocean communities, where smaller particles numerically comprise a comparatively greater component of the overall particle assemblage.

3.3. Absorption

In the model described by equation (5), the total absorption coefficient, $a(\lambda)$, is calculated by summing the contributions to absorption of individual seawater constituents (equation (3)). The absorption coefficient of water molecules is assumed constant and equal to reported values for pure water [*Pope and Fry*, 1997]. The absorption by particles and CDOM are treated as variables and are parameterized as functions of Chl.

3.3.1. Particle absorption. In surface waters of both regions, phytoplankton cells were the dominant component contributing to particulate absorption, even in spectral regions of weak pigment absorption. The spectrum of $a_p(\lambda)$ thus closely resembles typical phytoplankton absorption curves, with well-defined peaks near the principal absorption bands of chlorophyll *a*. Based upon methanol extractions of these samples, phytoplankton pigments contributed on average 81% and 74% to the total particulate absorption at light wavelengths of 440 and 555 nm, respectively. Detrital absorption, although a smaller percentage of particulate absorption, was highly correlated with both phytoplankton absorption ($r = 0.95$ at $\lambda = 440$ nm) and Chl ($r = 0.97$).

Particulate absorption varies nearly 2 orders of magnitude within our data set and is highly correlated with Chl (Figure

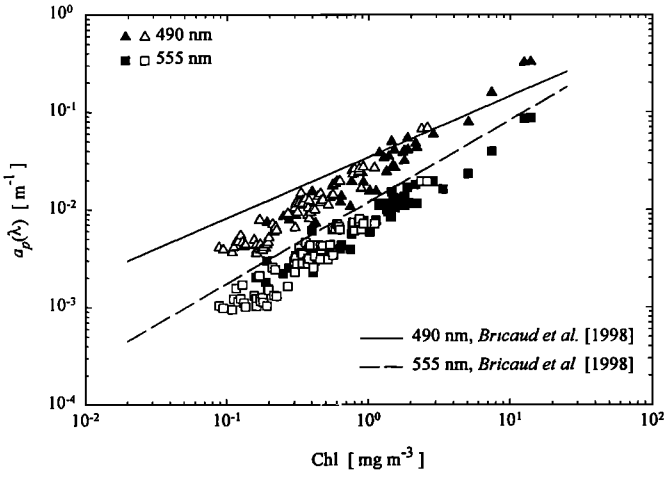

Figure 3. Particulate absorption coefficients at 490 and 555 nm as a function of chlorophyll concentration. Solid symbols represent surface data from the Ross Sea ($N = 73$); open symbols depict surface measurements from the APFZ ($N = 92$). For comparison, the lines illustrate the predicted relationship of the *Bricaud et al.* [1998] model developed from a large, geographically diverse data set collected from nonpolar waters.

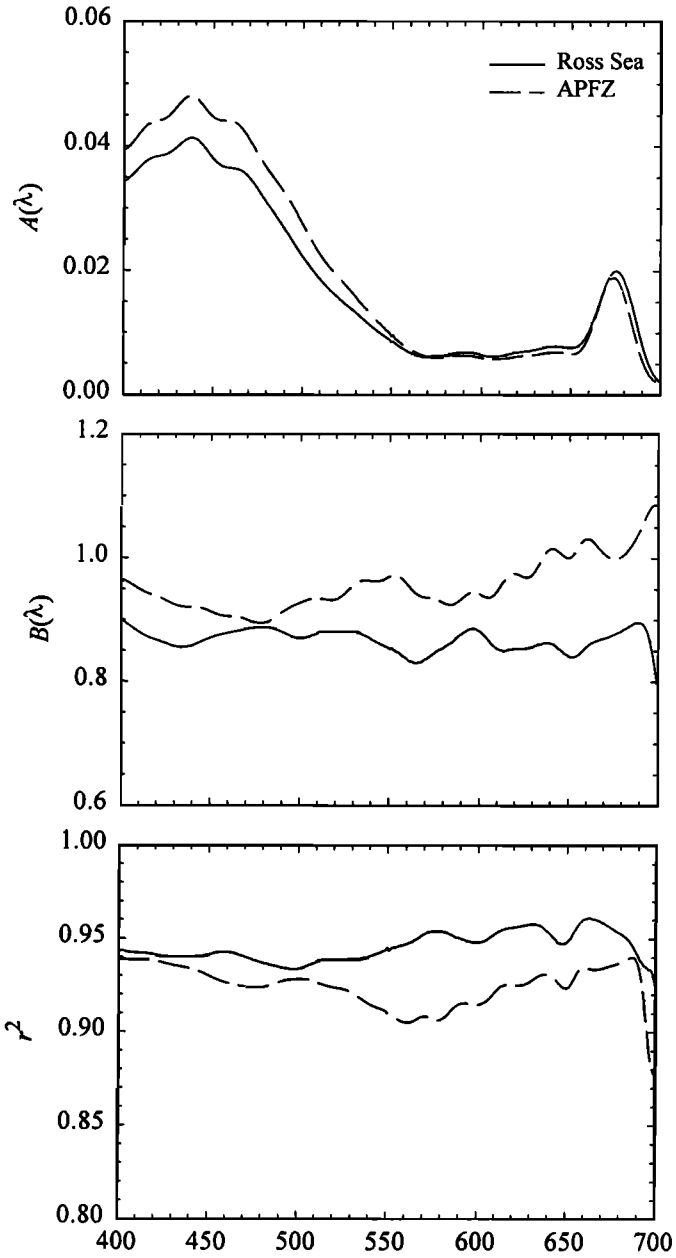

Figure 4. Spectral values of the numerical coefficients (top) A and (middle) B and (bottom) the coefficient of determination r^2, obtained for the power function describing the variability in particulate absorption coefficients as a function of Chl (equation (6)). All coefficients were obtained by linear regression on log-transformed data from the Ross Sea (solid lines, $N = 73$) and the APFZ (dashed lines, $N = 92$).

3). In both the Ross Sea and the APFZ, the relationship between $a_p(\lambda)$ and Chl is well described by a power function of the form

$$a_p(\lambda) = A(\lambda)\mathrm{Chl}^{B(\lambda)}, \quad (6)$$

where the coefficients $A(\lambda)$ and $B(\lambda)$ are empirically determined by linear regression on the log-transformed data. The fitted spectral values of these numerical coefficients, which are used as inputs to the reflectance model, indicate small yet significant differences in the average spectral shape of particulate absorption between the two regions (Figure 4). Values of $A(\lambda)$ are in close agreement within the spectral region of 550-700 nm, with differentiation between the two regions more pronounced at shorter wavelengths. At the blue absorption peak of chlorophyll a, the fitted value of $A(443)$ for the APFZ is 16% higher than for the Ross Sea, which is just significant (F test, $\alpha = 0.05$). The exponents obtained for equation (6), $B(\lambda)$, in the visible region are generally close to 1, indicating that the relationship between $a_p(\lambda)$ and Chl is approximately linear.

Comparison of our measurements with a model developed by using a similar parameterization of a large, geographically diverse data set obtained in nonpolar waters [*Bricaud et al.*, 1998] suggests that for Chl < 1, particulate absorption coefficients in Southern Ocean waters are significantly less than the "global" norm (by ~20-60%, depending upon Chl and wavelength). This is in agreement with previous observations that Chl-specific particulate absorption coefficients, $a^*_p(\lambda)$, are generally low in the Southern Ocean [*Mitchell and Holm-Hansen*, 1991; *Sosik et al.*, 1992]. Decreased values of a^*_p may result from a lesser contribution of detrital material to particulate absorption, reduced contributions to absorption by pigments other than chlorophyll, variability in absorption per unit chlorophyll a resulting from pigment packaging effects [e.g., *Morel and Bricaud*, 1981], or some combination of these factors. Our estimates of the average contribution of detrital absorption to a_p are very similar to the average contribution reported by Bricaud et al. (25-30%) for their measurements. The influence of pigment packaging can be assessed to a first order by examining the red absorption band of chlorophyll a near 676 nm, where the contribution of accessory pigments to absorption is generally small. In the APFZ, $a^*_p(676)$ averaged 0.019 ± 0.004 m^2 (mg Chl)$^{-1}$ and exhibited no clear trend with Chl (the exponent in equation (6), $B(676)$, has a value of 1, indicating a linear relationship between a_p and Chl). This number, when compared with commonly accepted values of in vivo Chl-specific absorption coefficients for unpackaged cellular material of 0.023-0.029 m^2 (mg Chl)$^{-1}$ [*Johnsen et al.*, 1994; *Moisan and Mitchell*, 1999], suggests small to moderate pigment packaging effects in this region. In contrast, within the Ross Sea $a^*_p(676)$ in general decreases with Chl (the exponent $B(676) = 0.87$). The model parameterization for this region predicts $a^*_p(676)$ to decrease systematically from a value of 0.026 to 0.014 m^2 (mg Chl)$^{-1}$ over a Chl range of 0.1 to 15 mg m^{-3}.

3.3.2. CDOM absorption. The oceanic CDOM pool is comprised of a complex mixture of organic compounds, each having a characteristic turnover time. These compounds originate from a number of sources, including terrestrial inputs, photochemical reduction-oxidation reactions, and biological processes such as cell lysis and degradation, exudation, and grazing. In Antarctic waters, terrigenous inputs of CDOM are generally negligible, and deep winter mixing is likely to limit the accumulation of a long-lived CDOM pool which can yield a background concentration independent of Chl [*Bricaud et al.*, 1981]. Biological sources of CDOM may covary with the Chl to some degree, but the correlation is expected to be weak, as these processes may be out of phase with phytoplankton biomass and production, and CDOM may have a relatively long residence time in surface waters.

The spectral shape of $a_{cdom}(\lambda)$ decreases in an approximate exponential fashion with increasing wavelength, and meas-

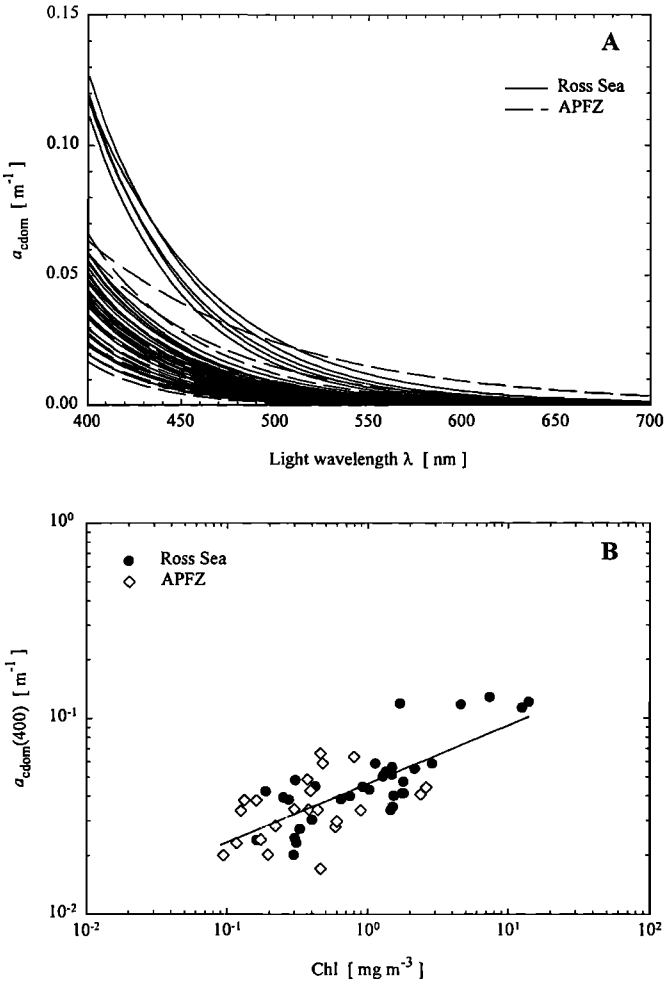

Figure 5. (a) Spectral absorption curves of colored dissolved organic material, $a_{cdom}(\lambda)$, from the Ross Sea (solid lines) and the APFZ (dashed lines). Spectra were obtained by fitting measured absorption curves to an exponential model (equation (7)). (b) Variations in $a_{cdom}(400)$ as a function of Chl. The solid line depicts the best fit regression, calculated by using the pooled data from both regions, and represents equation (8) in the text.

urements in the spectral region 300-600 nm were fitted to the model

$$a_{cdom}(\lambda) = a_{cdom}(\lambda_o)\, e^{-S(\lambda-\lambda_o)}, \quad (7)$$

where S is an empirical factor and λ_o is a reference wavelength. Considerable variability was observed in the magnitudes and shape of CDOM absorption spectra obtained from surface waters in both regions, with the highest values measured in high biomass Ross Sea waters dominated by *Phaeocystis* (Figure 5a). The value of the slope parameter, S, has been reported to vary between 0.010 and 0.020 nm^{-1} and is dependent upon the relative proportions of specific constituents comprising the CDOM pool [*Carder et al.*, 1989; *Roesler et al.*, 1989; *Kirk*, 1994]. The mean value of S for both regions in our data set is 0.0195 ± 0.004 nm^{-1}, and this was used in the reflectance model.

The magnitude of a_{cdom} at 400 nm varies 7.5 fold in the combined data set for the two regions and demonstrates a weak but significant correlation with Chl (Figure 5b). Accordingly, in the reflectance model $a_{cdom}(\lambda)$ is calculated from equation (7) by assuming a constant value of $S = 0.0195$ nm^{-1}, a reference wavelength of 400 nm, and the relation

$$a_{cdom}(400) = 0.046\,\mathrm{Chl}^{0.298}, \quad r^2 = 0.55, N = 55. \quad (8)$$

3.4. Backscattering

The total backscattering coefficient $b_b(\lambda)$ is partitioned into a constant contribution by water molecules, $b_{bw}(\lambda)$, and a varying contribution by the particle fraction, $b_{bp}(\lambda)$,

$$b_b(\lambda) = [b_{bw}(\lambda_o) + b_{bp}(\lambda_o)]\left(\frac{\lambda_o}{\lambda}\right)^{\gamma}, \quad (9)$$

where γ is a dimensionless parameter describing the spectral dependency of total backscattering relative to a reference wavelength, λ_o. We parameterize our model by using a reference wavelength of 555 nm.

3.4.1. Particle backscattering versus Chl. Particulate backscattering coefficients at 555 nm, calculated as $b_b(555) - b_{bw}(555)$, where $b_{bw}(555) = 0.00925$ m^{-1}, in surface waters of both regions varied from 0.00033 to 0.0098 m^{-1}, comprising 26% and 91% of the total backscattering coefficient, respectively, at this wavelength. In both regions, $b_{bp}(555)$ covaried with Chl, but the relation is significantly distinct between the two regions (Figure 6a):

Ross Sea

$$b_{bp}(555) = 0.001\ \mathrm{Chl}^{0.667}, \quad r^2 = 0.85, N = 67 \quad (10a)$$

APFZ

$$b_{bp}(555) = 0.004\ \mathrm{Chl}^{0.822}, \quad r^2 = 0.86, N = 27. \quad (10b)$$

The dominant contribution to particle backscattering in the ocean typically arises from small particles in the approximate size range 0.1 to 2 μm [*Morel and Ahn*, 1991; *Stramski and Kiefer*, 1991]. At a given Chl, the magnitude of particulate backscattering in the APFZ is significantly higher than in the Ross Sea. The reduced Chl-specific particulate backscattering observed in the Ross Sea suggests that Chl in this region is generally contained in larger particles which contribute comparatively less to backscattering, which is consistent with Coulter counter measurements of particle size distributions. Another possible factor contributing to this observation is that nonchlorophyllous particles that efficiently backscatter light, such as small sized detritus, are less abundant in the Ross Sea than the APFZ. For comparison, the model of *Morel* [1988], whose derivation did not include backscattering measurements, is also illustrated in Figure 6a. This model is generally inconsistent with our relationships but would perform well at moderate chlorophyll concentrations in the APFZ.

3.4.2. Spectral shape of backscattering. The spectral dependency of total backscattering, γ, also reflects a combination of the relative contributions by water and the particle component. The wavelength dependence of backscattering by water molecules varies as $\sim\lambda^{-4.3}$, while the spectral dependency of particulate backscattering is variable and dependent upon the composition of the particle assemblage. Previous models of backscattering have often assumed a constant wavelength dependence for b_{bp} which is relatively flat (λ^0 or λ^{-1}), although some recent efforts have allowed it to vary as a function of trophic status [*Carder et al.*, 1999; *Ciotti et al.*, 1999]. Our measurements in both regions indicate that the wavelength dependence of particulate backscattering

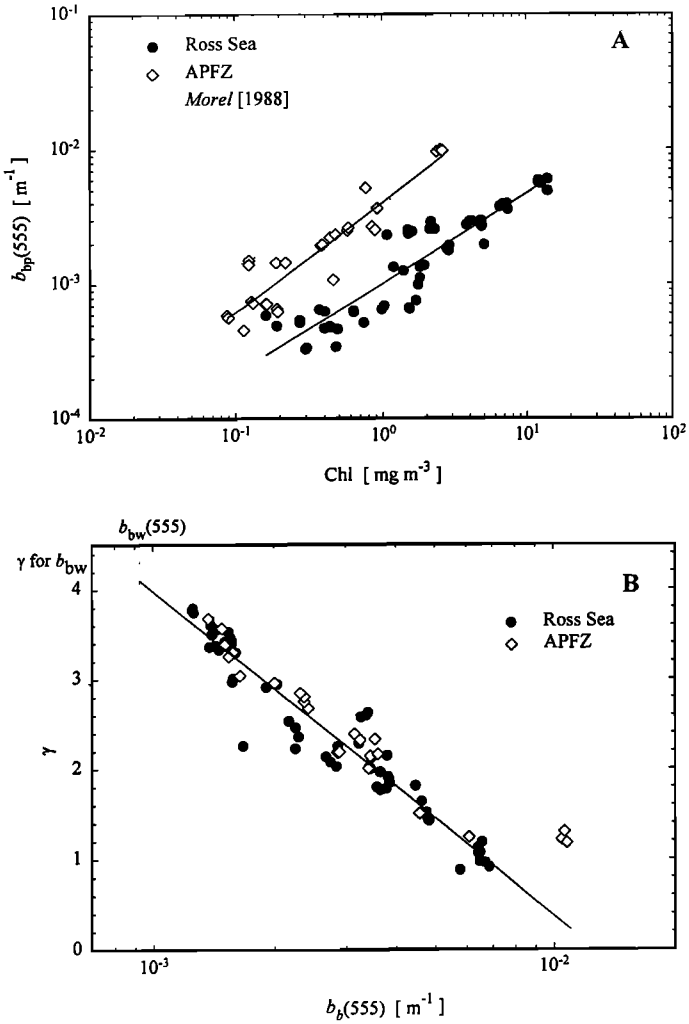

Figure 6. (a) Relationship between the particulate backscattering coefficient at 555 nm, $b_{bp}(555)$, and Chl for the Ross Sea and the APFZ. The solid lines represent the fitted equation (10) obtained for each region. For comparison, the relationship predicted by using the model of *Morel* [1988] is illustrated by the dotted line. The Morel model, formulated for the sum of chlorophyll plus pheopigments, was calculated by using the relation Chl = 0.76 (Chl + Pheo) developed from our data set. (b) Semilog plot depicting variability in the wavelength dependency of total backscattering γ and the backscattering coefficient at 555 nm. Pure seawater values for $b_b(555)$ and γ are indicated by the dotted lines. The solid line illustrates the fitted equation (11).

is variable, ranging from λ^{-3} to $\lambda^{-0.8}$, with a general tendency to decrease with increasing Chl. The greatest variability in b_{bp} spectral dependence occurs in low Chl waters, where the magnitude of b_{bp}, and thus its contribution to total backscattering, is low.

Owing to this last observation, in our model we chose to parameterize the slope of the total backscattering, rather than the slope of particulate backscattering. At low to moderate values of b_b, the parameter γ is strongly influenced by the contribution of water, and thus the observed variability in particle backscattering shape exerts a lesser influence on this parameter. As particulate backscattering increases, its contribution to γ also increases and variability in the wavelength dependence of $b_{bp}(\lambda)$ becomes more significant. For the combined data from both regions, the wavelength dependence of total backscattering is strongly correlated with the magnitude of backscattering at 555 nm (Figure 6b) through the relation

$$\gamma = -3.616 \log_{10} [b_b(555)] - 6.866, \quad r^2 = 0.93, N = 88. \quad (11)$$

For calculation of this regression, the three data points from the APFZ corresponding to very high $b_b(555)$ were not included. These three points represent repeated measurements from the same station at which elevated values of surface Chl remained from an earlier widespread bloom. This empirical equation combines the effects of varying contributions of water and the variable wavelength dependence of particle backscattering. The extrapolated value at $b_b(555) = b_{bw}(555)$ for this relationship yields $\lambda^{-4.10}$ for the wavelength dependence of pure seawater.

3.5. Parameterization of f/Q

The reflectance is related to the inherent optical properties of absorption and backscattering through the ratio $f(\lambda)/Q(\lambda)$. The parameters $f(\lambda)$ and $Q(\lambda)$ are both variable and depend in a complicated manner upon the solar zenith angle, the geo-

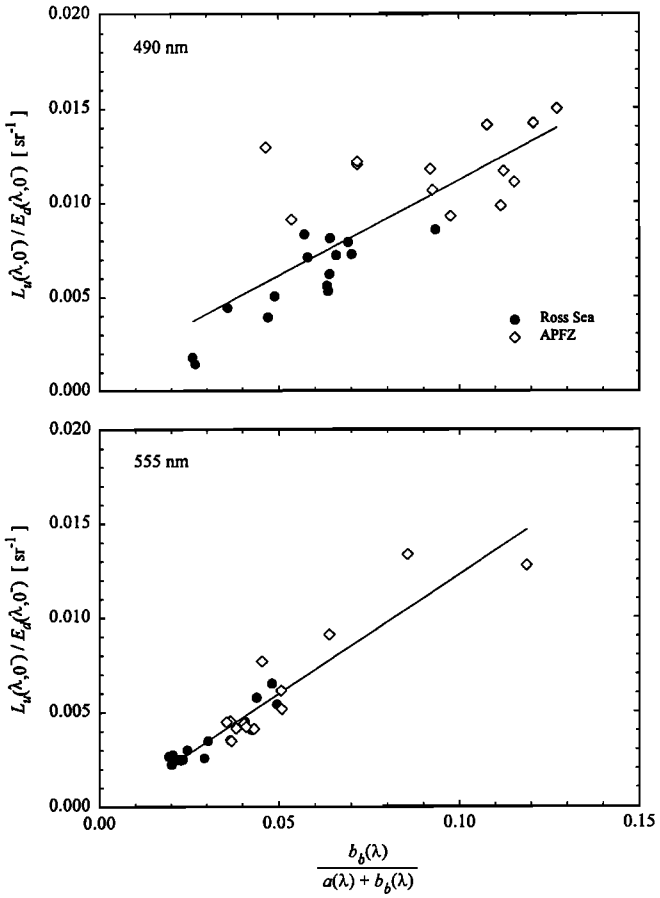

Figure 7. Relationship between measurements of the upwelling radiance to downwelling radiance ratio, L_u/E_d, and the ratio of backscattering to the sum of absorption and backscattering, $b_b/(a + b_b)$, for light wavelengths of (top) 490 and (bottom) 555 nm. The slope of the regression line is interpreted as representing the average value of the ratio f/Q (see equation (2) in the text).

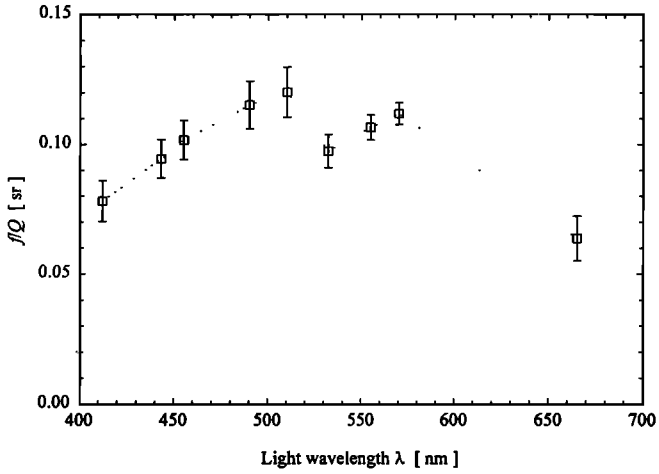

Figure 8. Spectral variations in the average value of $f(\lambda)/Q(\lambda)$ as computed by linear regression analysis on the relationships depicted in Figure 7, using the pooled data from both regions. The analysis was done at nine visible wavelengths corresponding to the spectral bands measured with the MER spectroradiometer. Error bars represent the standard error of the slope parameter.

metric structure of the radiance field, and on the seawater IOPs. Numerical studies suggest that f and Q vary in a manner such that the ratio f/Q may be more conservative than the individual parameters [*Morel and Gentili,* 1993]. To a first approximation, the behavior of this ratio can be examined by comparing subsurface radiometric measurements of the directional reflectance, L_u/E_d, with the ratio $b_b/(a+b_b)$ determined from concurrent measurements of inherent optical properties (see equation (2)). This comparison is graphically illustrated for two spectral regions in Figure 7 and, to our knowledge, represents the first empirical examination of this quantity utilizing actual field measurements. The results suggest that, within all spectral bands included in our measurements, the relationship between these quantities is approximately linear and thus implies a limited range in the ratio f/Q. This result may be attributable to the fact that our measurements were done at high latitudes and under usually overcast atmospheric conditions, thus resulting in a relatively restricted range of solar elevations and sky radiance distributions.

The slope parameter obtained by regression analysis can be considered as an average value of f/Q, and spectral variations in this slope are illustrated in Figure 8. These empirically determined values of f/Q vary approximately twofold and exhibit some wavelength dependency. The magnitudes lie within the range of reported values (~0.08 to 0.12) determined from Monte Carlo simulations for various combinations of solar zenith angles and radiance distributions [*Morel and Gentili,* 1993]. Considering the potential sources of error involved in the numerous measurements involved in this analysis (L_u, E_d, b_b, a_p, a_{cdom}), this general agreement with theoretical calculations is encouraging and lends confidence to the validity of the individual measurements. However, because of these uncertainties, it is difficult to ascertain whether the observed spectral behavior, such as the apparent decrease in $f(\lambda)/Q(\lambda)$ in the 530- and 670-nm bands, are real features.

4. Application of the Forward Model

By utilizing the parameterizations of the inherent optical properties in terms of Chl and the empirically determined estimates of f/Q, the model described by equation (5) can be used to compute the $R_{rs}(\lambda)$ spectra for various values of Chl.

4.1 Modeled Relationships Between $R_{rs}(\lambda)$ and Chl

Figure 9 illustrates model predictions, specific for each region, of the spectral remote sensing reflectance with surface Chl as a varying parameter. The model was run for Chl values which span the approximate range encountered in each region. Changes in the reflectance spectra with Chl clearly reveal the well-known patterns associated with the opposing

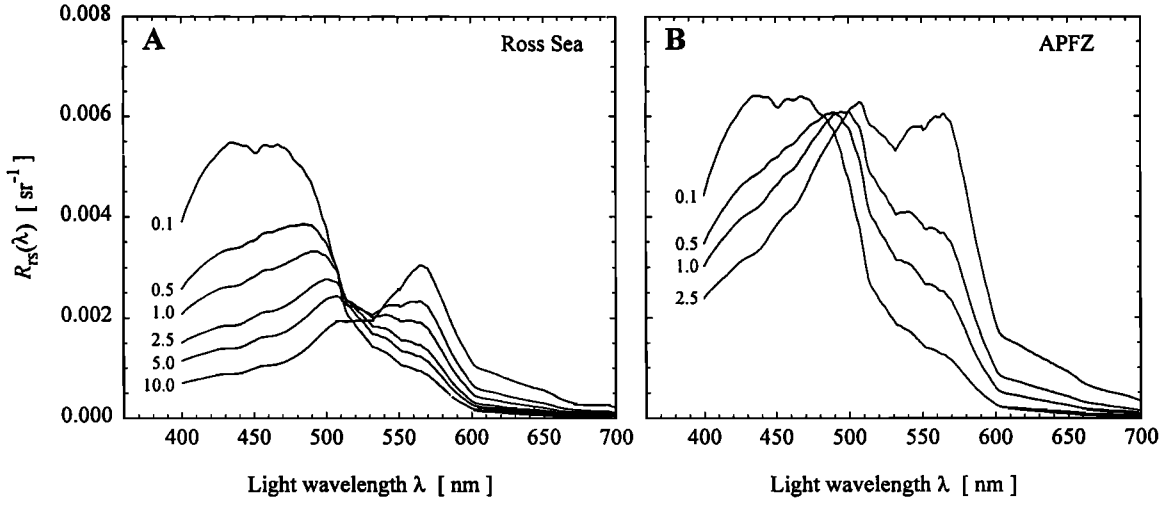

Figure 9. Model predictions of the remote sensing reflectance spectrum, $R_{rs}(\lambda)$, for (a) the Ross Sea and (b) the APFZ for varying chlorophyll concentration as indicated in the figure. Regional parameterizations of the dependence of absorption and backscattering coefficients on Chl were used as inputs to the model described in equation (5), in combination with empirical determinations of spectral variability in f/Q (Figure 8) and a constant value of $\kappa = 0.54$.

effects of a and b_b [e.g., *Gordon and Morel,* 1983]. In the blue spectral region the absorption by particles and CDOM exerts a dominant influence, and R_{rs} values decrease with increasing Chl. In the green spectral region, variability in backscattering with Chl is more important and reflectance exhibits an increase with increasing Chl. This interplay of absorption and backscattering results in a characteristic spectral "hinge point" in the reflectance spectra where increases in absorption and backscattering with Chl are such that the net effect is effectively balanced.

For a given value of Chl, the R_{rs} spectrum for the APFZ is significantly higher in magnitude than that predicted for the Ross Sea region, and the location of the hinge point is blue-shifted by about 30 nm. This demonstrates the strong influence that variability in the relationships between IOPs and Chl can have on the magnitude and shape of the R_{rs} spectrum. Within the Chl range 0–2.5 mg m^{-3}, the total absorption coefficient differs by less than 20% within all spectral regions; thus the primary source of this regional variability in the R_{rs} spectrum is the different relationships between backscattering and Chl.

The R_{rs} spectra computed by the model can be used for the estimation of Chl. By running the model at various Chl values, a library of $R_{rs}(\lambda)$ is generated which can then be compared with reflectance measurements made either in situ or from satellites. Chl can be estimated by iterative comparison of a measured R_{rs} spectrum with the library and finding the modeled spectrum which most closely matches the measured spectrum. This approach allows one to take full advantage of all available spectral information, as opposed to relying solely on ratios of a few spectral bands.

4.2 Comparison of the Model With Two-Band Empirical Algorithms

Empirical algorithms for predicting pigment concentration from reflectance have primarily utilized ratios of blue to green spectral bands. The NASA SeaWiFS program, for example, has used both Ocean Color 2-band (OC2) and Ocean Color 4-band (OC4) algorithms [*O'Reilly et al., 1998; O'Reilly et al.,* 2000] for global processing of SeaWiFS data. OC2 calculates Chl from a statistical relationship with the ratio $R_{rs}(490)/R_{rs}(555)$, while OC4 uses the maximum band ratio for the band combinations of 443/555, 490/555, and 510/555. Here we explore the relative influence of absorption and backscattering for the 490/555 band ratio. The regional differences in the parameterizations of backscattering and absorption with Chl results in regionally specific relationships between $R_{rs}(490)$, $R_{rs}(555)$, and their spectral ratio with Chl (Figure 10). In the APFZ, the spectral hinge point in the reflectance spectrum occurs around 490 nm, and thus R_{rs} in this spectral band shows little variability with Chl (Figure 10a). In contrast, within the Ross Sea region $R_{rs}(490)$ exhibits a systematic decrease with increased pigment concentrations. In both regions, $R_{rs}(555)$ increases with Chl, but the relationship clearly shows the regional distinction caused by the different backscattering parameterizations (Figure 10b).

When the spectral band ratio, $R_{rs}(490)/R_{rs}(555)$, is computed from our model (Figure 10c) the sigmoidal shape characteristic of previous semianalytical models is reproduced [e.g., *Morel,* 1988; *Gordon et al.,* 1988]. For waters with low Chl, both the Ross Sea and APFZ models converge to a clear water value of 6.595 for the ratio, which compares very well with the expected value of approximately 6.6. With increasing Chl, the relationship between $R_{rs}(490)/R_{rs}(555)$ and Chl diverges between the two regions. In the APFZ, the relative insensitivity of $R_{rs}(490)$ to Chl and larger magnitude of $R_{rs}(555)$ at a given Chl results in a faster decrease, relative to

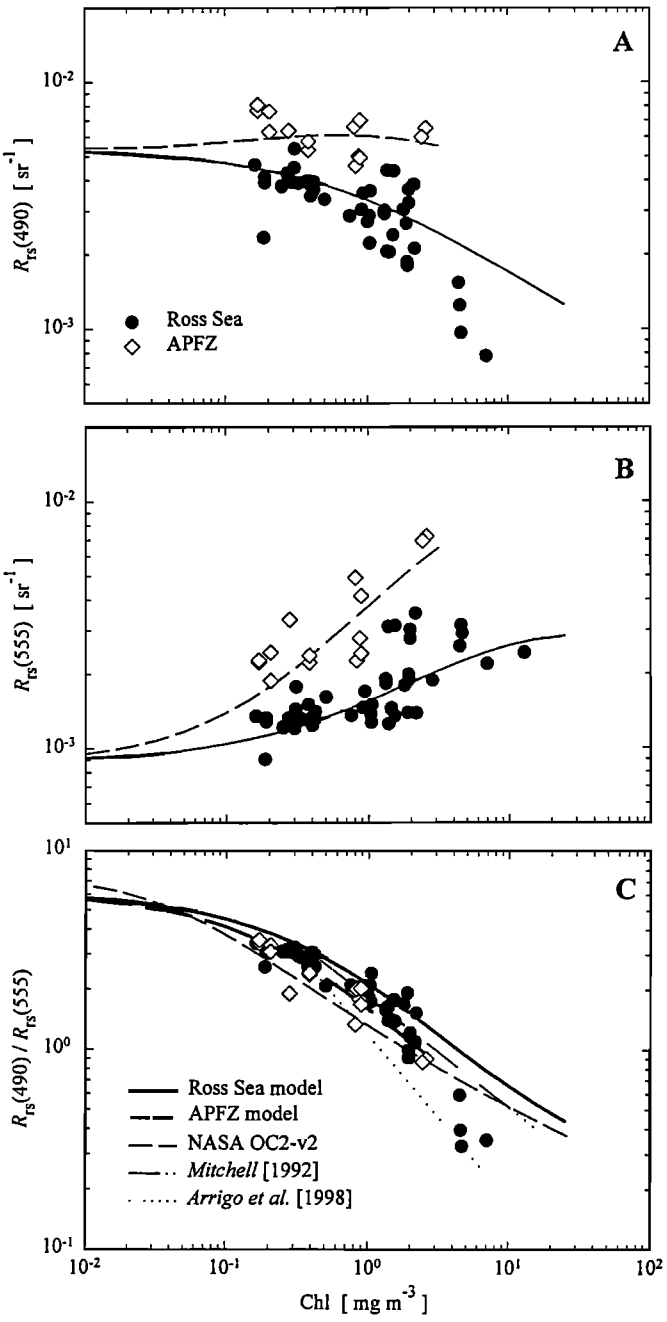

Figure 10. The relationship between R_{rs} and Chl at light wavelengths of (a) 490 and (b) 555 nm. Symbols represent radiometric measurements obtained with the MER spectroradiometer in the Ross Sea and the APFZ. Lines represent the relationship predicted from the model by using specific parameterizations of the inherent optical properties for the Ross Sea (solid lines) and the APFZ (dashed lines). (c) Modeled relationships between the spectral band ratio $R_{rs}(490)/R_{rs}(555)$ and Chl obtained in the Ross Sea and the APFZ. Also depicted are empirical algorithms including the NASA OC2 [*O'Reilly et al.,* 1998] version 2 algorithm, the Antarctic algorithm of *Mitchell* [1992], and the *Arrigo et al.* [1998] algorithm for the Ross Sea.

Ross Sea, in the ratio with Chl. The Ross Sea model does a poor job of accurately reproducing the sharp decrease in the reflectance ratio observed at the highest Chl, however. These stations are characterized by the presence of the highest soluble absorption, which is not easily represented by a Chl-dependent parameterization.

In Figure 10c, the modeled relationships between the band ratio $R_{rs}(490)/R_{rs}(555)$ and Chl are compared with previous empirical algorithms. For a given value of Chl, the NASA OC2-v2 model predicts a significantly lower value of the reflectance ratio. As a result, the application of this model to these regions leads to a consistent underestimation of Chl by approximately a factor of 2 (range 35-65%). The *Mitchell* [1992] Antarctic algorithm falls in between the predicted Ross Sea and APFZ relationships for Chl < 3 mg m^{-3}. The *Arrigo et al.* [1998] model for the Ross Sea does well at high and low Chl but does poorly for Chl between 0.4 and 3 mg m^{-3}.

It is of interest to examine the individual contributions of absorption and backscattering to variability in the $R_{rs}(490)/R_{rs}(555)$ versus Chl relationship. As the magnitude of b_b is small in relation to a (usually less than 10% in our data set), the contribution of backscattering to the denominator in equation (2) can be neglected and the ratio of R_{rs} at two arbitrary wavelengths expressed as the product of three spectral ratios:

$$\frac{R_{rs}(\lambda_1)}{R_{rs}(\lambda_2)} = \left(\frac{f(\lambda_1)/Q(\lambda_1)}{f(\lambda_2)/Q(\lambda_2)}\right)\left(\frac{a(\lambda_2)}{a(\lambda_1)}\right)\left(\frac{b_b(\lambda_1)}{b_b(\lambda_2)}\right). \quad (12)$$

Spectral variations in $f(\lambda)/Q(\lambda)$ are small and exhibit no apparent trend with Chl in our data set (but see *Morel and Gentili* [1993]); thus as a first approximation the influence of this term on the reflectance band ratio can be neglected. Measurements of the ratio of absorption at 555 to 490 nm have a maximal value approaching 3 for waters containing 0.1 mg m^{-3} Chl and show a systematic decrease with increasing Chl with no significant differences between Ross Sea and APFZ (Figure 11a). As the 555:490 absorption ratio for the particulate and dissolved fractions do not exhibit any trend with Chl, this behavior principally results from changes in the relative contribution of water to the total absorption coefficient.

Similar to absorption, the spectral band ratio describing the contribution of backscattering (in this case, 490 to 555 nm) to $R_{rs}(490)/R_{rs}(555)$ is maximal in clear waters and declines with increasing Chl (Figure 11b). The overall range of variability in this ratio is less than that observed for absorption; however, in contrast to absorption, there appears to be a clear regional separation in which consistently lower values are observed in the APFZ for a given Chl. As the relationship of the spectral slopes of backscattering to the magnitude of b_b is nearly the same between the two regions (Figure 6b), the lower ratio of $b_b(490)/b_b(555)$ primarily results from the fact that for a given Chl the magnitude of $b_b(\lambda)$ is greater in the APFZ.

The product of the absorption and backscattering ratio, which is proportional to the R_{rs} band ratio, is illustrated in Figure 11c. The contribution of backscattering effectively increases the dynamic range of the absorption band ratio. Using the parameterizations of absorption and backscattering components with Chl, the relative contributions of variability in backscattering and absorption to the expected changes in the R_{rs} band ratio with Chl can be calculated. Let $R^{(x)}$ denote

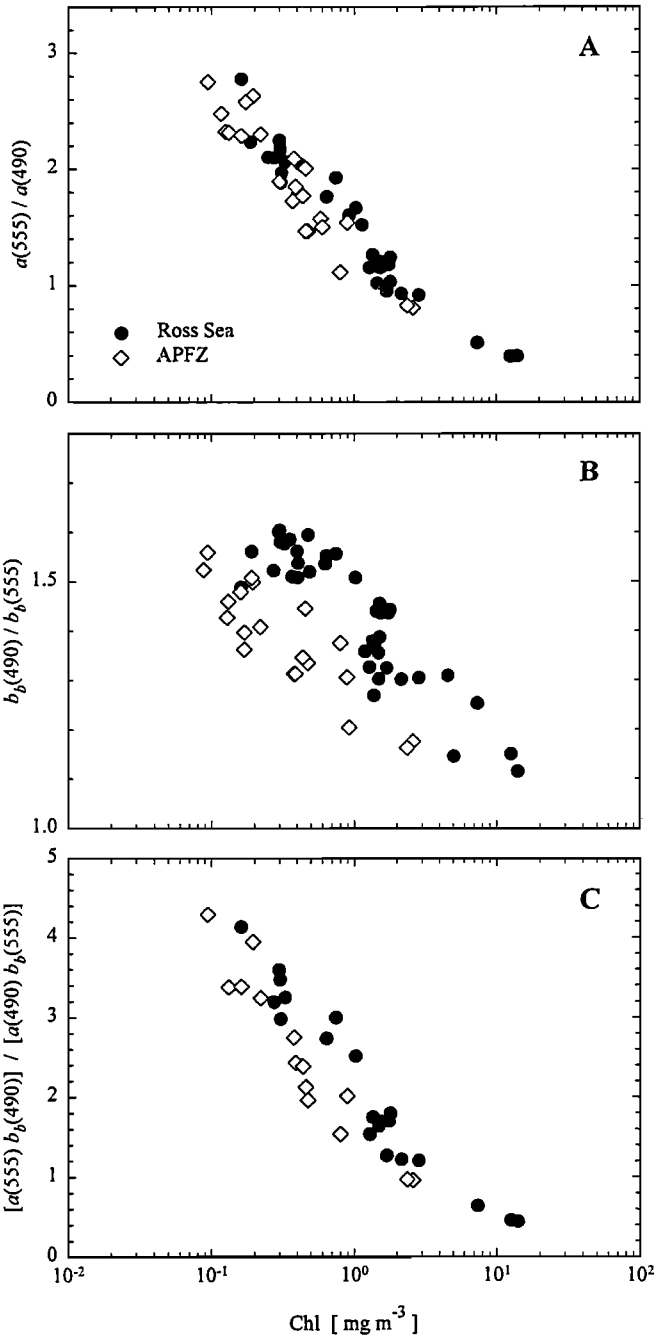

Figure 11. Measurements of the spectral band ratios for (a) absorption at 555:490 nm, (b) backscattering at 490:555 nm, and (c) their product as a function of Chl for the Ross Sea (solid circles) and APFZ (open diamonds).

the value of $R_{rs}(490)/R_{rs}(555)$ for an arbitrary Chl of x. We can similarly define for each concentration of Chl the spectral ratio of $a(555)/a(490)$ as $a^{(x)}$, and the spectral ratio of $b_b(490)/b_b(555)$ as $b_b^{(x)}$. Following equation (12), the modeled change in the remote sensing reflectance spectral ratio which occurs as Chl changes from x_1 to x_2 mg m^{-3} can then be expressed as

$$\frac{R^{(x_2)}}{R^{(x_1)}} = \frac{a^{(x_2)}}{a^{(x_1)}}\frac{b_b^{(x_2)}}{b_b^{(x_1)}}. \quad (13)$$

Because we assume that the ratio $f(\lambda)/Q(\lambda)$ exhibits no de-

Table 1. Model Results for Partitioning of Changes in the Spectral Band Ratio $R_{rs}(490)/R_{rs}(555)$ into Individual Contributions of Changes in the Absorption Ratio, $a(555)/a(490)$, and the Backscattering Ratio, $b_b(490)/b_b(555)$

Variable	x_1	x_2	Change, % $(100 \cdot (x_1 - x_2)/x_1)$	Contribution to $\Delta[R_{rs}(490)/R_{rs}(555)]$, %
		Ross Sea		
Chl, mg m^{-3}	0.16	14.32		
$a(555)/a(490)$	2.52	0.44	-82.4	83.7
$b_b(490)/b_b(555)$	1.58	1.13	-28.6	16.3
$R_{rs}(490)/R_{rs}(555)$	3.98	0.50	-87.4	
		APFZ		
Chl, mg m^{-3}	0.07	2.59		
$a(555)/a(490)$	2.87	0.82	-71.5	76.7
$b_b(490)/b_b(555)$	1.54	1.05	-31.7	23.3
$R_{rs}(490)/R_{rs}(555)$	4.43	0.86	-80.6	

For each region, the model was run for the minimum (x_1) and maximum (x_2) surface chlorophyll concentration observed within the data set. All optical parameters are dimensionless ratios. The fourth column represents the percentage change calculated for the optical ratio over the range in Chl, and the fifth column is the calculated contribution (in percent) to the modeled change in the R_{rs} band ratio.

pendency with Chl (Fig. 7), it cancels out in this analysis. Table 1 illustrates an example of this partitioning analysis for both the Ross Sea and APFZ using specific absorption and backscattering parameterizations of the components for each region. The model was run at two values of Chl, representing the minimum and maximum surface concentrations observed in our field studies, to generate calculated spectral band ratios values for reflectance, absorption, and backscattering. The results demonstrate that a decrease in the ratio of absorption at 555 to 490 nm is the dominant mechanism contributing to changes in the $R_{rs}(490)/R_{rs}(555)$ ratio with increasing Chl, but the contribution of changes in the spectral backscattering ratio are not negligible (~20%). For example, in the Ross Sea surface Chl varies nearly 100-fold, resulting in an 87% decrease in the predicted R_{rs} spectral band ratio. This decrease results from a combination of a greater than fivefold decrease in the ratio of $a(555)/a(490)$ and a 29% decrease in $b_b(490)/b_b(555)$. The decrease in the absorption ratio results from a reduced contribution of water at 490 nm, relative to 555 nm, as absorption by particles and dissolved materials increase. The decrease in the backscattering spectral ratio reflects flattening of the backscattering spectrum, in response to both increases in the contribution of particle scattering relative to water and a general flattening of the particulate backscattering spectrum.

As was indicated in the methods section, fluorometric and HPLC analyses of water samples in the APFZ show discrepancies in the estimates of Chl. In this study, we chose to use fluorometric estimates of chlorophyll *a* to ensure consistency with widely accepted values of the Chl-specific absorption coefficient of phytoplankton (<0.03 m^2 (mg Chl)$^{-1}$ in the red absorption peak of chlorophyll *a*). Nevertheless, it is worthwhile to briefly comment on how our results would be influenced by utilization of HPLC estimates of Chl. First, the relationship between particulate absorption and Chl would display larger differences between the Ross Sea and APFZ regions, in contrast to little or no regional distinction observed by using fluorometric Chl (Figure 3). Second, the separation between the two regions in terms of the backscattering versus Chl relationship would become much more pronounced than that shown in Figure 6a. Because of these trends, the relationships of the blue-to-green reflectance ratio and the corresponding absorption-to-backscattering ratio with Chl would show even greater differences between the Ross Sea and APFZ than presently depicted in Figure 10c and Figure 11c, respectively.

5. Conclusions

Improvements in technological instrumentation and measurement protocols, combined with the growing availability of large bio-optical data sets, are resulting in increasingly refined statistical algorithms for describing the empirical relationships between oceanic reflectance and phytoplankton pigment concentrations. In concert with these developments, insight into the mechanisms which drive these empirical relationships has increased through the development of semianalytical models describing the links between Chl and the inherent optical properties. At present, empirical algorithms generally provide better or similar accuracy in Chl retrieval than semianalytical approaches [*O'Reilly et al.*, 1998]. A major advantage of the latter models, however, is the ability to develop understanding of the large variability observed in ocean color empirical relationships, including differentiation in bio-optical relationships between various regions of the global ocean.

The present model for predicting ocean reflectance in Southern Ocean waters relies upon well-known descriptions relating R_{rs} to the inherent optical properties of absorption and backscattering and Chl-dependent parameterizations based on a comprehensive suite of in situ optical measurements. Semianalytical models, such as the model described here, have several potential uses. With this approach, libraries of expected reflectance spectra for various chlorophyll concentrations can be generated with high spectral resolution for specific oceanic regions. These libraries can be used to estimate Chl as well as other optical and biogeochemical

variables and will be useful in exploring alternative ocean color algorithms to take advantage of multiple spectral bands which are expected to be available on future satellite sensors. For example, the use of a forward model in combination with the IOPs versus Chl relationships can be used in the training of neural networks to interpret ocean color [e.g., *Gross et al.*, 2000].

We have utilized our reflectance model to examine regional variability in the R_{rs} versus Chl relationship for two regions of the Southern Ocean. Previous attempts to explain regional differentiation in bio-optical relationships, including the distinct differences between the Southern Ocean and other oceanic regions [e.g., *Mitchell*, 1992], have primarily focused on the role of absorption. For several reasons, the potential role of backscattering has been examined to a much lesser degree. Our measurements demonstrate that changes in absorption spectrum have the dominant influence (>75%) on driving the overall blue to green R_{rs} ratio versus Chl relationship. However, although backscattering has a smaller influence on modifying the reflectance ratio than do changes in absorption, our results indicate that backscattering can be important for causing regional differentiation in reflectance ratio algorithms. As the relationship between absorption and Chl is very similar for the two regions investigated in this study, the primary phenomena leading to regional differentiation in the R_{rs} versus Chl relationship is the larger backscattering per unit Chl in the APFZ.

Notation

z water depth, m.

λ light wavelength, nm.

$R_{rs}(\lambda)$ remote sensing reflectance, sr^{-1}.

$L_w(\lambda)$ water-leaving nadir radiance, W m^{-2} sr^{-1} nm^{-1}.

Chl fluorometric chlorophyll a concentration, mg m^{-3}.

N/V particle concentration within a size class of width 0.25 μm, m^{-3}.

$R(\lambda)$ irradiance reflectance, dimensionless.

$E_u(\lambda)$, $E_d(\lambda)$ upwelling and downwelling plane irradiance, W m^{-2} nm^{-1}.

$f(\lambda)$ parameter relating reflectance to the ratio $b_b/(a+b_b)$, dimensionless.

$Q(\lambda)$ ratio of upwelling irradiance to nadir radiance, sr.

$L_u(\lambda)$ upwelling nadir radiance, W m^{-2} sr^{-1} nm^{-1}.

$a(\lambda)$ absorption coefficient, m^{-1}.

$a_w(\lambda)$ absorption coefficient of pure water, m^{-1}.

$a_p(\lambda)$ absorption coefficient of particles, m^{-1}.

$a_{cdom}(\lambda)$ absorption coefficient of colored dissolved organic matter, m^{-1}.

$b_b(\lambda)$ backscattering coefficient, m^{-1}.

$b_{bw}(\lambda)$ backscattering coefficient of pure seawater, m^{-1}.

$b_{bp}(\lambda)$ backscattering coefficient of particles, m^{-1}.

$A(\lambda)$, $B(\lambda)$ numerical coefficients for describing the relationship between a_p and Chl (equation (5)).

S slope describing the wavelength dependence of a_{cdom}, nm^{-1}.

γ spectral dependency of b_b, dimensionless.

Acknowledgments. Financial support for this research was provided by NASA Oceanography and SIMBIOS Programs (NAG5-7100, NAS5 97130) and NSF (OPP 98-02836) as part of the U.S. JGOFS Antarctic Environment Southern Ocean Process Study. We thank J. Wieland and B. Bichnevicious for assistance in the collection of field data, M. Kahru for providing data processing codes, and the staff of Antarctic Support Associates as well as the officers and crews of the R/V *Nathaniel B. Palmer* and the R/V *Roger Revelle* for logistical support. Fluorometric pigment data were provided by Walker Smith. This is JGOFS contribution 538.

References

Arrigo, K. R., D. H. Robinson, D. L. Worthen, B. Schieber, and M. P. Lizotte, Bio-optical properties of the southwestern Ross Sea, *J. Geophys. Res.*, *103*, 21,683-21,695, 1998.

Austin, R. W., Inherent spectral radiance signals of the ocean surface, in *Ocean Color Analysis, SIO Ref. 74-10*, pp. 2.1-2.20, Scripps Inst. of Oceanogr., La Jolla, Calif., 1974.

Bianchi, T. S., C. Lambert, and D. C. Biggs, Distribution of chlorophyll *a* and phaeopigments in the northwestern Gulf of Mexico: A comparison between fluorometric and high-performance liquid chromatography measurements, *Bull. Mar. Sci.*, *56*, 25-32, 1995.

Bricaud, A., A. Morel, and L. Prieur, Absorption by dissolved organic matter of the sea (yellow substance) in the UV and visible domains, *Limnol. Oceanogr.*, *26*, 43-53, 1981.

Bricaud, A., A. Morel, M. Babin, K. Allali, and H. Claustre, Variations of light absorption by suspended particles with chlorophyll *a* concentration in oceanic (case 1) waters: Analysis and implications for bio-optical models, *J. Geophys. Res.*, *103*, 31,033-31,044, 1998.

Carder, K. L., R. G. Steward, G. R. Harvey, and P. G. Ortner, Marine humic and fulvic acids: Their effects on remote sensing of ocean chlorophyll, *Limnol. Oceanogr.*, *34*, 68-81, 1989.

Carder, K. L., F. R. Chen, Z. P. Lee, S. K. Hawes, and D. Kamykowski, Semianalytic Moderate-Resolution Imaging Spectrometer algorithms for chlorophyll *a* and absorption with bio-optical domains based on nitrate depletion-temperatures, *J. Geophys. Res.*, *104*, 5403-5421, 1999.

Ciotti, Á. M., J. J. Cullen, and M. R. Lewis, A semi-analytical model of the influence of phytoplankton community structure on the relationship between light attenuation and ocean color, *J. Geophys. Res.*, *104*, 1559-1578, 1999.

Cleveland, J. S., Regional models for phytoplankton absorption as a function of chlorophyll *a* concentration, *J. Geophys. Res.*, *100*, 13,333-13,344, 1995.

Garver, S., D. A. Siegel, and B. G. Mitchell, Variability in near-surface particulate absorption spectra: What can a satellite ocean color imager see?, *Limnol. Oceanogr.*, *39*, 1349-1367, 1994.

Gordon, H. R., and A. Morel, Remote assessment of ocean color for interpretation of satellite visible imagery, a review, in *Lecture Notes on Coastal and Estuarine Studies*, 113 pp., Springer-Verlag, New York, 1983.

Gordon, H. R., O. B. Brown, R. H. Evans, J. W. Brown, R. C. Smith, K. S. Baker, and D. K. Clark, A semianalytic radiance model of ocean color, *J. Geophys. Res.*, *93*, 10,909-10,924, 1988.

Gross, L., S. Thiria, R. Frouin, and B. G. Mitchell, Artificial neural networks for modeling the transfer function between marine reflectance and phytoplankton pigment concentration, *J. Geophys. Res.*, *105*, 3483-3495, 2000.

Johnsen, G., O. Samset, L. Granskog, and E. Sakshaug, In vivo absorption characteristics in 10 classes of bloom-forming phytoplankton: Taxonomic characteristics and responses to photoadaptation by means of discriminant and HPLC analysis, *Mar. Ecol. Prog. Ser.*, *105*, 149-157, 1994.

Kirk, J. T. O., *Light and Photosynthesis in Aquatic Ecosystems*, 509 pp., Cambridge Univ. Press, New York, 1994.

Kishino, M., M. Takahashi, N. Okami, and S. Ichimura, Estimation of the spectral absorption coefficients of phytoplankton in the sea, *Bull. Mar. Sci.*, *37*, 634-642, 1985.

Knap, A., A. Michaels, A. Close, H. Ducklow, and A. Dickson (Eds.), Protocols for the Joint Global Ocean Flux Study (JGOFS) core measurements, *JGOFS Rep.19*, 170 pp., UNESCO, Paris, 1994.

Maffione, R. A., and D. R. Dana, Instruments and methods for measuring the backward-scattering coefficient of ocean waters,*Appl. Opt.*, *36*, 6057-6067, 1997.

Mitchell, B. G., Algorithms for determining the absorption coefficient of aquatic particulates using the quantitative filter technique (QFT), in *Ocean Optics X*, edited by R. Spinrad, Proc. Int. Soc. Opt. Eng., 10, 137-148, 1990.

Mitchell, B. G., Predictive bio-optical relationships for polar oceans and marginal ice zones, *J. Mar. Syst.*, *3*, 91-105, 1992.

Mitchell, B. G., and O. Holm-Hansen, Bio-optical properties of Antarctic Peninsula waters: Differentiation from temperate ocean models, *Deep Sea Res.*, *38*, 1009-1028, 1991.

Mitchell, B. G., and M. Kahru, Algorithms for SeaWiFS developed with the CalCOFI data set, *CalCOFI Rep. 39*, 26 pp., Calif. Coop. Oceanic Fish. Invest., La Jolla, Calif., 1998.

Mobley, C. D., *Light and Water: Radiative Transfer in Natural Waters*, 592 pp., Academic, San Diego, Calif., 1994.

Moisan, T. A., and B. G. Mitchell, Photophysiological acclimation of *Phaeocystis antarctica* Karsten under light limitation, *Limnol. Oceanogr.*, *44*, 247-258, 1999.

Moore, J. K., M. R. Abbot, J. G. Richman, W. O. Smith, T. J. Cowles, K. H. Coale, W. D. Gardner, and R. T. Barber, SeaWiFS satellite ocean color data from the Southern Ocean,*Geophys. Res. Lett.*, *26*, 1465-1468, 1999.

Morel, A., Optical modeling of the upper ocean in relation to its biogenous matter content (case 1 waters), *J. Geophys. Res.*, *93*, 10,749-10,768, 1988.

Morel, A., and Y-H. Ahn, Optics of heterotrophic nanoflagellates and ciliates: A tentative assessment of their scattering role in oceanic waters compared to those of bacterial and algal cells,*J. Mar. Res.*, *49*, 1-26, 1991.

Morel, A., and A. Bricaud, Theoretical results concerning light absorption in a discrete medium, and application to specific absorption of phytoplankton, *Deep Sea Res., Part A*, *28*, 1375-1393, 1981.

Morel, A., and B. Gentili, Diffuse reflectance of oceanic waters: Its dependence on Sun angle as influenced by the molecular scattering contribution, *Appl. Opt.*, *30*, 4427-4438, 1991.

Morel, A., and B. Gentili, Diffuse reflectance of oceanic waters, II, Bidirectional aspects, *Appl. Opt.*, *32*, 6864-6879, 1993.

Mueller, J. L., and R. W. Austin, Ocean optics protocols for SeaWiFS validation, revision 1, *NASA Tech. Memo.*, *25(104566)*, 67 pp., 1995.

Neveux, J., et al., Comparison of chlorophyll and phaeopigment determinations by spectrophotometric, fluorometric, spectrofluorometric, and HPLC methods, *Mar. Microb. Food Webs*, *4*, 217-238, 1990.

O'Reilly, J. E., S. Maritorena, B. G. Mitchell, D. A. Siegel, K. L. Carder, S. A. Garver, M. Kahru, and C. McClain, Ocean color chlorophyll algorithms for SeaWiFS, *J. Geophys. Res.*, *103*, 24,937-24,953, 1998.

Pegau, S., J. S. Cleveland, W. Doss, C. D. Kennedy, R. A. Maffione, J. L. Mueller, C. C. Trees, A. D. Weidemann, W. H. Wells, and J. R. V. Zaneveld, A comparison of methods for the measurement of the absorption coefficient in nature waters,*J. Geophys. Res.*, *100*, 13,201-13,220, 1995.

Pope, R. M., and E. S. Fry, Absorption spectrum (380-700 nm) of pure water, II, Integrating cavity measurements,*Appl. Opt.*, *36*, 8710-8723, 1997.

Preisendorfer, R. W., Application of radiative transfer theory to light measurements in the sea, *Monogr. 10*, pp. 11-30, Int. Union of Geod. and Geophys., Paris, 1961.

Roesler, C. S., M. J. Perry, and K. L. Carder, Modeling in situ phytoplankton absorption from total absorption spectra in productive inland waters, *Limnol. Oceanogr.*, *34*, 1510-1523, 1989.

Sarmiento, J. L., and J. C. Orr, Three-dimensional simulations of the impact of Southern Ocean nutrient depletion on atmospheric CO_2 and ocean chemistry, *Limnol. Oceanogr.*, *36*, 1928-1950, 1991.

Sarmiento, J. L., T. M. C. Hughes, R. J. Stouffer, and S. Manabe, Simulated response of the ocean carbon cycle to anthropogenic climate warming, *Nature*, *393*, 245-249, 1998.

Siegel, D. A., M. C. O'Brien, J. C. Sorensen, D. A. Konnoff, and E. Fields, BBOP data processing and sampling procedures, *U.S. JGOFS Plann. Rep.19*, 80 pp., U.S. Joint Global Ocean Flux Study Proj. Off., Woods Hole, Mass., 1995.

Smith, W. O., Jr., R. F. Anderson, J. K. Moore, L. Codispoti and J. M. Morrisson, The U.S. Southern Ocean Joint Global Ocean Flux Study: An introduction to AESOPS, *Deep-Sea Research II*, in press, 2000.

Sosik, H. M., M. Vernet, and B. G. Mitchell, RACER3: A comparison of particulate absorption properties between high- and mid-latitude waters, *Antarct. J. U. S.*, *27*, 162-164, 1992.

Stramski, D., and D. A. Kiefer, Light scattering by microorganisms in the open ocean, *Prog. Oceanogr.*, *28*, 343-383, 1991.

Trees, C. C., R. R. Bidigare, and J. M. Brooks, Distribution of chlorophylls and phaeopigments in the northwestern Atlantic Ocean,*J. Plankton Res.*, *8*, 447-458, 1986.

B. G. Mitchell, R. A. Reynolds, D. Stramski, Scripps Institution of Oceanography, University of California San Diego, La Jolla, CA 92093. (gmitchell@ucsd.edu; reynolds@ocean.washington.edu; stramski@mpl.ucsd.edu)

(Received July 2, 1999; revised September 7, 2000; accepted November 6, 2000.)